ISSN 0957-4484

NANOTECHNOLOGY

VOLUME 23 NUMBER 11 23 MARCH 2012

iopscience.org/nano

Featured article

The application of graphene as electrodes in electrical and optical devices

G Jo, M Choe, S Lee, W Park, Y H Kahng and T Lee

IOP Publishing

Nanotechnology **23** (2012) 112001 (19pp) doi:10.1088/0957-4484/23/11/112001

TOPICAL REVIEW

The application of graphene as electrodes in electrical and optical devices

Gunho Jo[1,5], Minhyeok Choe[2], Sangchul Lee[3], Woojin Park[2], Yung Ho Kahng[4] and Takhee Lee[1]

[1] Department of Physics and Astronomy, Seoul National University, Seoul 151-747, Korea
[2] School of Materials Science and Engineering, Gwangju Institute of Science and Technology, Gwangju 500-712, Korea
[3] Department of Nanobio Materials and Electronics, Gwangju Institute of Science and Technology, Gwangju 500-712, Korea
[4] Research Institute for Solar and Sustainable Energies, Gwangju Institute of Science and Technology, Gwangju 500-712, Korea

E-mail: tlee@snu.ac.kr

Received 11 October 2011, in final form 27 January 2012
Published 28 February 2012
Online at stacks.iop.org/Nano/23/112001

Abstract
Graphene is a promising next-generation conducting material with the potential to replace traditional electrode materials such as indium tin oxide in electrical and optical devices. It combines several advantageous characteristics including low sheet resistance, high optical transparency and excellent mechanical properties. Recent research has coincided with increased interest in the application of graphene as an electrode material in transistors, light-emitting diodes, solar cells and flexible devices. However, for more practical applications, the performance of devices should be further improved by the engineering of graphene films, such as through their synthesis, transfer and doping. This article reviews several applications of graphene films as electrodes in electrical and optical devices and discusses the essential requirements for applications of graphene films as electrodes.

(Some figures may appear in colour only in the online journal)

1. Introduction

Since its discovery in 2004, graphene has attracted tremendous interest due to its advantageous material properties, including high charge mobility, transparency, mechanical strength and flexibility [1–8]. Accordingly, graphene is expected to play a crucial role as a transparent electrode in electronic and optoelectronic devices [9–11]. Transparent electrodes are an essential element of numerous devices, such as displays (liquid crystal displays, cellular phones, e-paper, etc), light-emitting diodes and photovoltaic devices, used by billions of people [12]. In particular, it is estimated that 290 million displays will be produced in 2014 (figure 1 [13]), and thus the demand for transparent electrodes will significantly increase. Today, indium tin oxide (ITO) is by far the dominant material used in transparent electrodes (3 billion dollars worth in 2010 with a 20% growth rate through 2013) [10, 14]. However, the price of ITO is continuously increasing due to the limited supply of indium [10, 15, 16], and ITO is difficult to apply in flexible devices because of its brittleness under bending [10, 15]. These issues have stimulated numerous developments aimed at searching for alternative transparent electrode materials. Several types of new transparent electrode materials may potentially replace ITO, including metallic nanowires [17, 18], carbon nanotubes (CNTs) [19, 20], conductive polymers such as poly(3,4-ethylenedioxythiophene):poly(styrenesulfonate)

[5] Present address: Mechanical and Aerospace Engineering, Princeton University, Princeton, NJ 08544, USA.

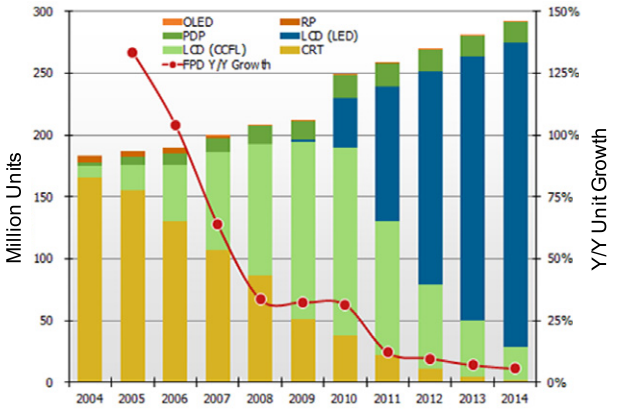

Figure 1. The flat panel display and transparent conductor market: OLED, organic light-emitting diode; RP, rear-projection; PDP, plasma display panel; LCD, liquid crystal display; CCFL, cold cathode fluorescent lamp; CRT, cathode ray tube; FPD, flat panel display. (Source: display search 'Quarterly Advanced Global TV shipment and Forecast Report'.)

(PEDOT:PSS) [21, 22] and graphene films [11, 23, 24]. Among these, graphene is particularly interesting because it has been successfully synthesized on a large scale as a good conducting and transferable film [25–30]. Already, pioneering works have reported a roll-to-roll production of 30-in graphene films grown by chemical vapor deposition that are superior to common transparent electrodes and other alternatives in terms of resistance and transparency [31]. Table 1 summarizes the key features of graphene (unoptimized and optimized) compared with other materials such as ITO [10, 32], Ag nanowires [33], CNTs [34] and PEDOT:PSS [35]. The advantageous properties of using graphene as a transparent electrode are essential when considering realistic applications. To this end, applications of graphene as electrodes in a wide range of devices including field-effect transistors [36], organic memories [37], molecular junction devices [38], touch screens [31], liquid crystal displays [39], light-emitting diodes [40–42] and organic solar cells [43, 44] have been reported. However, to ensure such applications, graphene films need to be further improved by engineering through synthesis [45–48], transfer [49, 50], doping [31, 51, 52] and tuning of their work functions [53, 54]. Regarding these aspects, this review surveys several techniques to prepare graphene films and highlights the essential requirements for electrode applications of graphene films. This review explains how the properties of graphene can be modified to produce more efficient electrodes. Finally, several applications of graphene as electrodes in electrical and optical devices are presented, and perspectives are also discussed.

2. Transparent conductive graphene

2.1. Graphene preparation

Graphene has been prepared by several techniques, including: (i) precipitation on a silicon carbide surface (figure 2(a)) [55], (ii) mechanical exfoliation from graphite (figure 2(b)) [1], (iii) chemically converted graphene from solution-phase graphene oxide (figure 2(c)) [56], and (iv) growth by chemical vapor deposition (CVD) on catalytic metal surfaces (figure 2(d)) [31]. The size and properties of a graphene layer depend on the method used for its preparation. The de Heer group reported the heat treatment of SiC in a vacuum or in an inert atmosphere to form a graphene layer on the SiC surface [57], which is a result of the evaporation of silicon atoms from the SiC surface and the resultant segregation of carbon atoms on the surface (figure 2(a)). It had been expected that this method would be suitable for the preparation of high-quality graphene; however, the size of a single domain of uniform layer thickness has not exceeded several micrometers. Geim and his co-workers successfully isolated graphene by mechanical exfoliation with Scotch tape [1]. Although this mechanical exfoliation approach is quite simple and the material properties of the obtained samples are good compared to those obtained by other methods, it is not realistic to obtain large-area and high-yield graphene films through this method. However, this exfoliation method will remain the method of choice for fabricating proof-of-concept devices [58].

In 2006, the Ruoff group demonstrated a solution-based process for producing single-layer graphene [59, 60]. The method relies on the chemical modification of graphite to produce a water-dispersible intermediary, graphite oxide. After oxidation by Hummers' method [61], graphene oxide becomes a layered stack of puckered sheets with AB stacking, which completely exfoliates upon the addition of mechanical energy [62]. Graphene oxide itself is not conducting, but the graphitic network can be substantially restored by thermal annealing or through treatment with chemical reducing agents. Therefore, the performance of graphene-oxide-based devices may be attributed to several factors: (i) reduction of oxygen on the graphene oxide flakes does not completely restore the π-conjugation in the films, and (ii) the vacuum filtration or spin-coating methods used to prepare reduced graphene oxide films lead to stacked graphene flakes and thus significant flake-to-flake resistance. Further electrical enhancement of reduced graphene oxide film can be achieved by chemical doping and/or a hybrid approach with other conducting materials such as carbon nanotubes [63] and metal grids [30].

Precipitation on a silicon carbide surface and mechanical exfoliation techniques are not suitable for large-scale fabrication of devices. In contrast, chemically converted graphene from solution-phase graphene oxide and CVD-grown graphene layers allow large-scale graphene integration with other materials. Although generally the film quality made by the latter two methods is inferior to the former two methods, the structural and electrical improvement of the graphene film can be made by modified CVD techniques and chemical doping [31, 64, 65]. In particular, a large-scale synthesis of graphene films on Ni or Cu layers by CVD is expected to enable various macroscopic applications such as transparent conducting films useful for flexible/stretchable electronics [25, 66]. To date, various transfer processes

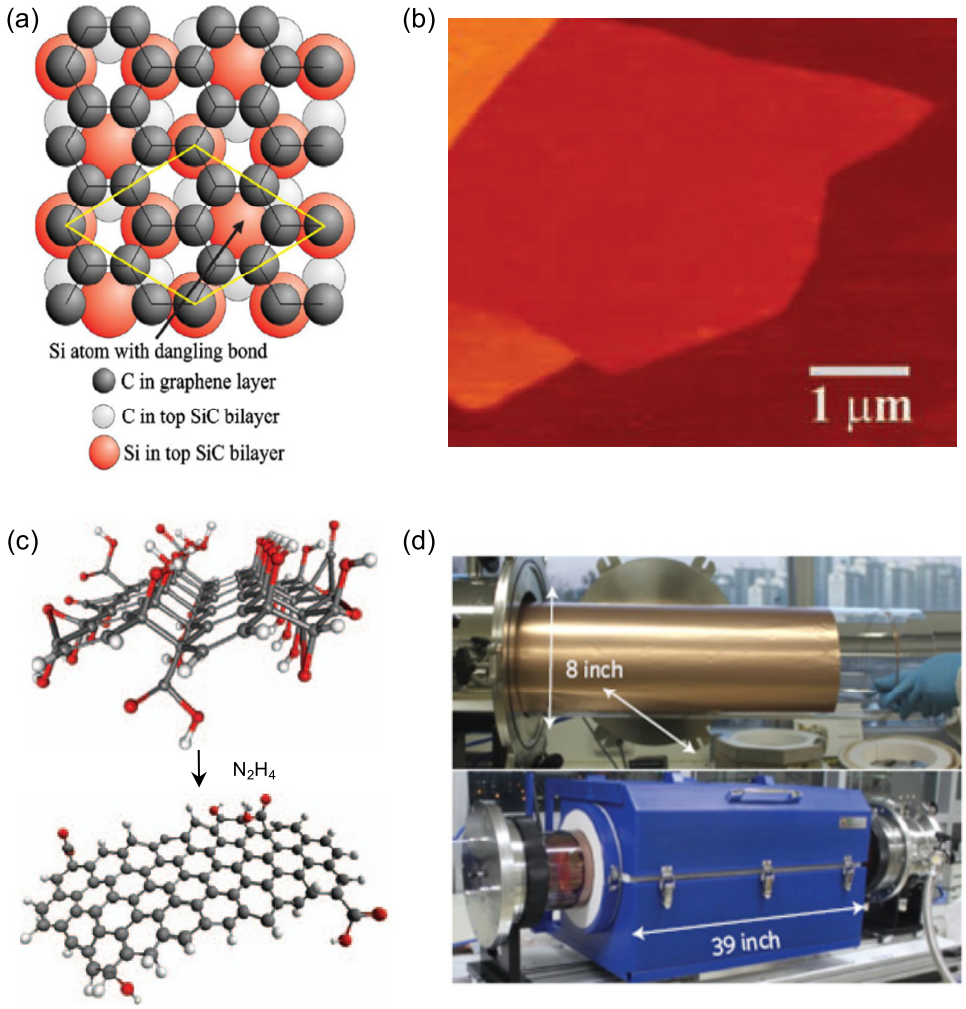

Figure 2. Four major preparation techniques for graphene films. (a) Epitaxial graphene on SiC(0001). Reproduced with permission from [51], Copyright 2008 American Physical Society. (b) AFM image of mechanically exfoliated graphene from of HOPG by using adhesive tape. Reproduced with permission from [1], Copyright 2004 American Association for the Advancement of Science (AAAS). (c) Chemically converted graphene from the solution phase (carbon in gray, oxygen in red and hydrogen in white). Reproduced with permission from [52], Copyright 2009 Nature Publishing Group. (d) Photograph shows the CVD setup with an 8 in wide tubular quartz reactor. Reproduced with permission from [31], Copyright 2010 Nature Publishing Group.

Table 1. Comparison of graphene (unoptimized and optimized) with other materials such as ITO, Ag nanowires, CNTs and PEDOT:PSS.

Material	$T(\%)$	R_S ($\Omega/\square$)	Status	Issue
ITO [32]	>85	15–30	Standard	Cost, brittle, corrosion by salts or acids, slow vacuum process
Ag nanowire [33]	>80	0.4–116	Commercialized, emerging	Roughness, environmental stability, haze, light scattering
CNT [34]	90	50	Emerging	High resistance, doping stability, roughness
PEDOT:PSS [35]	80	100	Limited use	Electrical/environmental stability, color tinge
Graphene [25, 27, 40] (unoptimized)	85	400 or more	Emerging	High resistance, doping stability
Graphene [31] (optimized)	85	Less than 30	Emerging	More doping up to few $\Omega/\square$, doping stability

of CVD-graphene films have been introduced. High yield and large-scale graphene transfer can be achieved using a polymer coating such as polymethyl methacrylate (PMMA) or polydimethylsiloxane (PDMS) as a provisional rigid support, which allow us to prevent folding or tearing of the graphene during etching of the metal catalyst [29, 67].

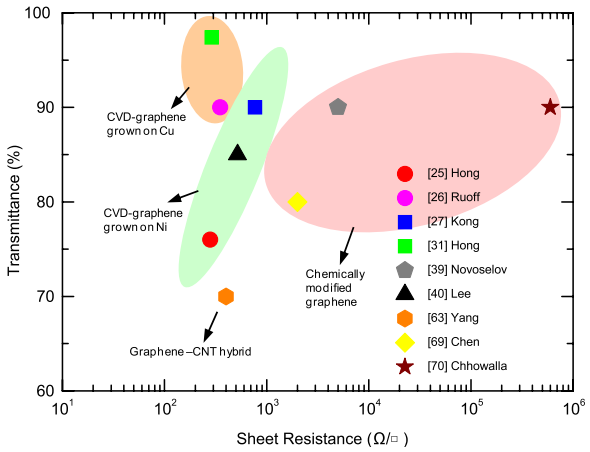

Figure 3. Sheet resistance and transmittance of graphene films reported from several groups.

Interestingly, the flexibility of the graphene and copper foils further allows efficient etching and transfer processes that use a cost- and time-effective roll-to-roll production method [31]. Although large-area graphene films can be prepared by solution-based processes and the CVD method, CVD-grown graphene films have the advantage that show approximately one order of magnitude less sheet resistance than solution-processed graphene films, making them more attractive for applications in high-performance electronic devices and transparent electrodes. Figure 3 shows the sheet resistance versus transmittance of graphene films reported from several groups [25, 27, 31, 39, 40, 63, 68–70]. To apply graphene materials as transparent electrodes, they should have low sheet resistance and high transmittance on a large scale. It is known that reduced graphene oxide leads to stacked graphene flakes, thus showing relatively lower uniformity than CVD-grown graphene films, particularly synthesized on Cu foil. In this sense, CVD-grown graphene would be preferable to that produced by other methods, while with reduced graphene oxide produced by solution processing it is simple and easy to prepare large-area graphene films. Therefore, graphene films created by these two methods are actively used as transparent electrodes in various device applications.

2.2. Optoelectronic properties

The utility of graphene films in applications such as transparent electrodes is largely governed by two critical parameters, sheet resistance and visible-light transmission, with each application having its own unique requirements. Either of these properties can be individually tuned to the desired value by changing the thickness of the graphene film. The sheet resistance is reduced as the graphene film becomes thicker, but the transmission is also reduced as the thickness increases. An effective transparent conductor should have high electrical conductivity combined with low absorption of visible light. Thus, an appropriate quantitative measure of the performance of transparent conductors is the ratio of the electrical conductivity σ to the visible absorption coefficient α,

$$\sigma/\alpha = -\frac{1}{R_s \ln(T+R)} \quad (1)$$

where R_s is the sheet resistance in ohms per square, T is the total visible transmission and R is the total visible reflectance [71]. Therefore, the value σ/α is a figure of merit used to rate transparent conductors. A large value of σ/α indicates good performance of transparent conductors.

Figure 4(a) shows the transmittance loss of CVD-synthesized graphene films due to increasing film thickness with increasing growth time [40]. Moreover, the sheet resistance and transmittance of graphene films are reduced with an increase in growth time (figure 4(b)). The transmittance (at 450 nm wavelength) and sheet resistance of three different graphene films (growth time = 3, 5, 7 min) were found to be 90% and ∼850 Ω/□, 87% and ∼620 Ω/□, 85% and ∼520 Ω/□, respectively. In addition, the optical transmittances and the sheet resistances of the graphene films synthesized at three different growth temperatures are summarized in figures 4(c) and (d) [43]. Figure 4(a) shows the representative transmittances of graphene films synthesized at three different growth temperatures: 800, 900 and 1000 °C. The inset in this figure shows the transmittance to be 90.7 ± 1.5%, 88.8 ± 2.2% and 86.9 ± 1.2% at a wavelength of 515 nm according to the growth temperature. The plot of mobility versus resistance shown in figure 4(d) was obtained by taking the statistical means and standard deviations of synthesized films at each growth temperature. As expected, the higher-temperature-grown, thicker graphene films were less transparent and had lower sheet resistance. Specifically, graphene films prepared at growth temperatures of 800 °C, 900 °C and 1000 °C showed sheet resistances of 1730 ± 600 Ω/□, 990 ± 400 Ω/□ and 610 ± 140 Ω/□ and mobilities of 660 ± 270 $cm^2\ V^{-1}\ s^{-1}$, 1030 ± 440 $cm^2\ V^{-1}\ s^{-1}$ and 1180 ± 260 $cm^2\ V^{-1}\ s^{-1}$, respectively.

2.3. Engineering of graphene

High conductivity and low optical absorption make graphene an attractive material for a transparent conductive electrode. Graphene films that have high conductivity and low optical loss can be engineered using several methods to achieve: (1) an improvement of graphene quality, (2) doping of graphene films, and (3) surface modification of graphene electrodes.

2.3.1. Chemical doping of graphene films. Graphene is a two-dimensional material composed of a single atomic layer of sp^2-bonded carbon atoms. To improve the conductivity of graphene films, the carrier concentration of the carbon layer must be adjusted by shifting the Fermi level of graphene's zero-gap band structure away from the Dirac point, where the density of states is zero (figure 5(a)) [72]. The desired rigid band shift can be induced by chemical doping [31, 72–74], electrostatic gating [75], a metal contact [76] or dipole formation [45, 77], resulting in the modulation of graphene's

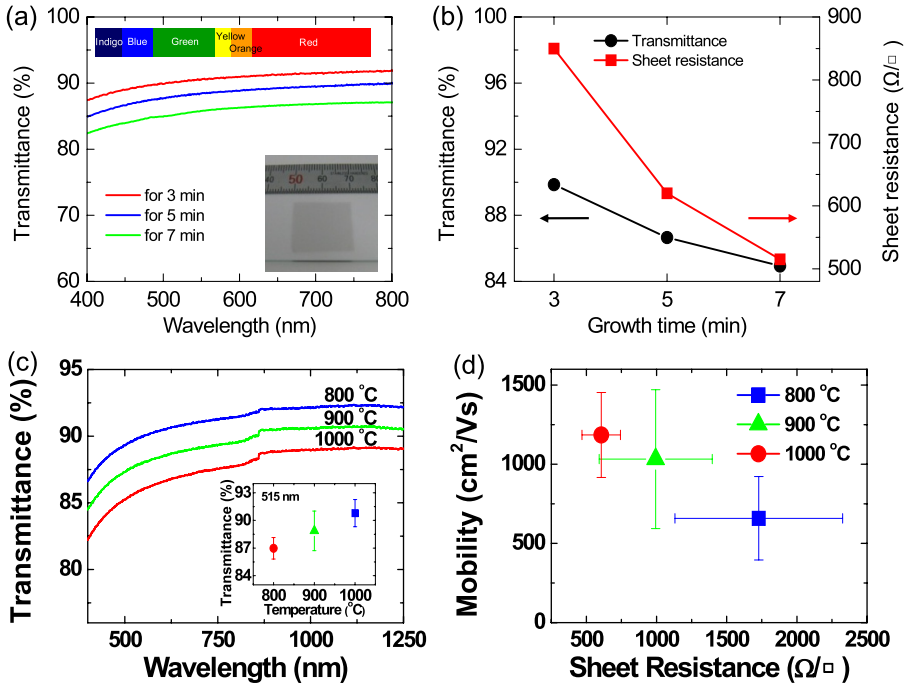

Figure 4. (a) Transmittance characteristics of graphene films prepared at different growth times of 3, 5 and 7 min. The inset shows a photograph of a centimeter-scale graphene film on a glass substrate. (b) Transmittance and sheet resistance of graphene films as a function of the growth time. (c) Transmittance spectra of graphene films with different growth temperatures of 800, 900 and 1000 °C. (d) Mobility versus sheet resistance of graphene films synthesized at different growth temperatures. (a), (b) Reproduced with permission from [36], Copyright 2010 IOP Publishing Ltd. (c), (d) Reproduced with permission from [39], Copyright 2010 Elsevier.

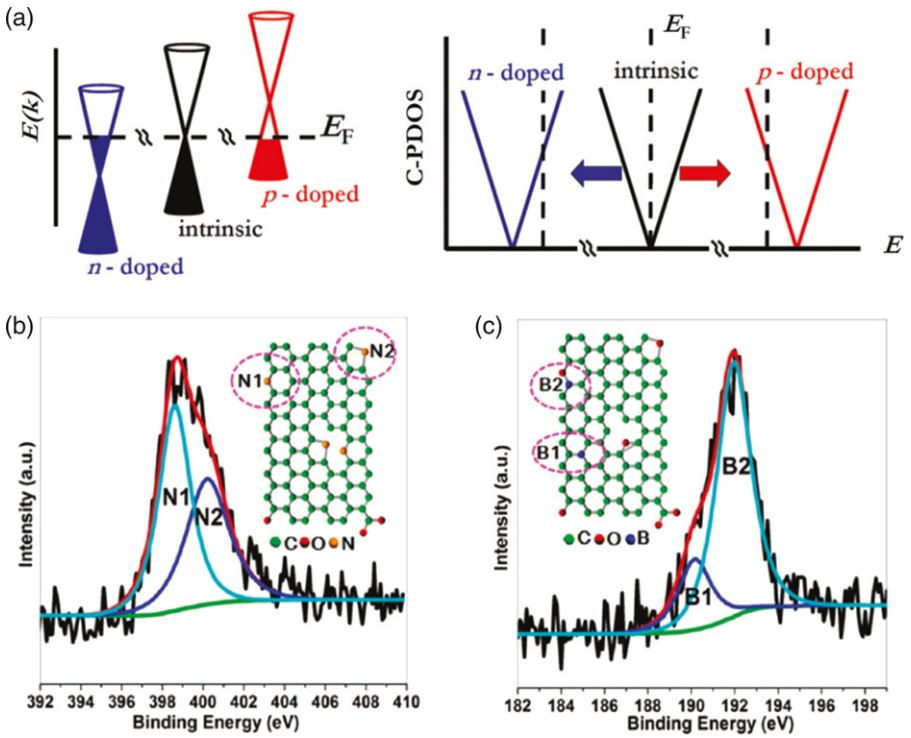

Figure 5. (a) $E(k)$ dispersion relation for graphene. Electrons (or holes) transferred to graphene shift the Fermi level away from the Dirac point. Reproduced with permission from [66], Copyright 2011 American Chemical Society. (b) N 1s XPS spectrum of the N-doped graphene. Inset: schematic structure of the binding conditions of N in a graphene lattice showing the pyridinic N (N1) and pyrrolic N (N2). (c) B 1s XPS spectrum of B-doped graphene. Inset: schematic structure of the binding conditions of B in a graphene lattice showing BC3 (B1) and BC2O (B2). (b), (c) Reproduced with permission from [75], Copyright 2011 American Chemical Society.

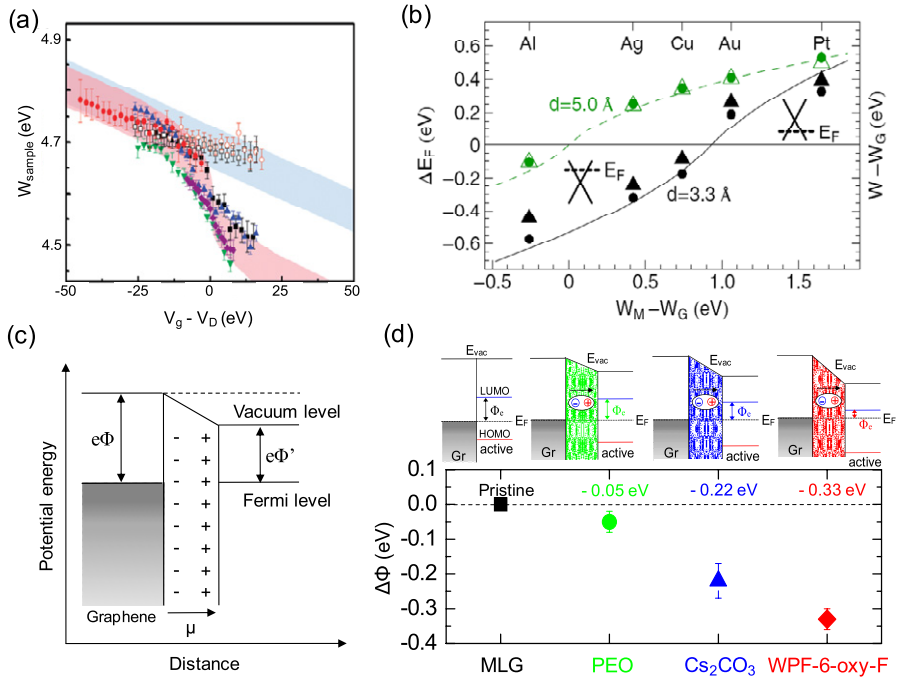

Figure 6. (a) Work function of the graphene surface (W_{sample}) versus the gate voltage minus the charge neutral gate voltage ($V_g - V_D$). Single-layer graphene samples show larger work function changes (shaded in red) while bilayer graphene samples exhibit fewer changes (shaded in blue). The filled green, red and purple symbols are single-layer graphene data taken in air. Other data were taken in a dry nitrogen environment. Reproduced with permission from [77], Copyright 2009 American Chemical Society. (b) Calculated Fermi energy shift with respect to the conical point, ΔE_F (dots), and change in the work function, $W - W_G$ (triangles), as a function of $W_M - W_G$ (W_M is the metal work function and W_G is the graphene work function). The insets illustrate the position of the Fermi level with respect to the conical point. Reproduced with permission from [78], Copyright 2008 American Physical Society. (c) Scheme for the formation of dipole layer on graphene and its effect on reducing the work function of graphene. (d) Control of work function with various dipole layers such as PEO, Cs_2CO_3 and WPF-6-oxy-F. Φ_e is the electron injection barrier between the graphene electrode and the LUMO of the active. Reproduced with permission from [49] Copyright 2010, American Institute of Physics.

conductive properties or work function. For example, hole (p) or electron (n) doping can be achieved by using elements such as B or N [78–81], which can be directly substituted into the carbon lattice during the growth of the layers to donate or remove electrons from the delocalized p_z-band (figure 5(b)) [81]. The N species in N-doped graphene are pyridinic N and pyrrolic N, which are formed predominately by substituting a carbon atom with N along in-plane edges or defect sites because such carbon atoms are much more chemically active than those within the plane of perfect graphene. Similarly, the B 1s XPS spectrum in figure 5(b) shows that the binding conditions of B in a B-doped graphene lattice are met by a B–C bond and B–O bond in BC_3 (B1) and BC_2O (B2), respectively.

Besides the use of direct substitution of elements to dope graphene samples, graphene can also be doped through the adsorption of chemical species on its surface. For example, by immersing graphene films in $AuCl_3$ solution [51, 54], Au particles can be formed on the surface of the film by the spontaneous reduction of metal ions (hole doping process), which gives rise to an up-shift in the surface potential and conductivity. Nitric acid (HNO_3) is another example of a molecular adsorbate that can be used to effectively p-dope graphene films [31]. P-doping with HNO_3 clearly reduces the sheet resistance of graphene films to values as low as ∼30 Ω/□ with ∼90% optical transmittance. In addition, the work function of graphene films changes by ∼130 meV with increasing doping time. Indeed, the modulation of sheet resistance and work function by doping is very important in enhancing the performance and efficiency of various electrical and optical devices based on graphene electrodes.

2.3.2. Tuning of the work function. Recent experimental studies have demonstrated that work-function engineering is possible by shifting the Fermi level of graphene's band structure via an electric field [75], metal contact [76] or dipole formation [53, 82] in addition to doping. Because the band alignment of two different materials is determined by their respective work functions, control over the graphene work function is the key to reducing the contact barriers of graphene electrode devices such as transistors [36], light-emitting diodes [40] and solar cells [53, 82]. For example, Yu *et al* [83] applied scanning Kelvin probe microscope techniques (which can map the surface potential variation of a sample surface relative to that of a metallic tip) to back-gated graphene devices and demonstrated that the work function can be controlled over a wide range of values by the Fermi level shift due to the electric-field-induced modulation of carrier concentration. The data regarding the work function of the graphene surface (W_{sample}) versus the gate voltage minus the charge neutral gate voltage ($V_g - V_D$) are shown in figure 6(a). The authors have found that the work functions of graphene

films can be tuned by an electric field over the range of 4.5–4.8 eV for single-layer graphene and 4.65–4.75 eV for bilayer graphene under ambient and dry nitrogen conditions. In addition, the intrinsic work functions were estimated to be 4.57 ± 0.05 eV and 4.69 ± 0.05 eV for undoped single-layer and bilayer graphene films, respectively.

The work function of graphene can also be modified with metal contacts. Giovannetti *et al* [84] reported that the use of metal contacts on graphene caused the Fermi level to move away from the conical points in graphene, resulting in doping with either electrons or holes. By calculating the Fermi energy shift with respect to the conical point, ΔE_F (dots), and the change in the work function $W - W_G$ (triangles), as a function of $W_M - W_G$, the difference in work function between a clean metal and graphene can be determined as shown in figure 6(b) [76]. The lower (black) and the upper (green) results are for the equilibrium (∼3.3 Å) and a larger (5.0 Å) separation of graphene and the metal surface, respectively. One would assume that graphene is doped with electrons if $W_G > W_M$ and doped with holes if $W_G < W_M$. The crossover point from n- to p-type doping would then occur at $W_M = W_G$. The results obtained at the equilibrium separation ($d \sim 3.3$ Å) of the graphene sheet and the metal surfaces show that this is clearly not the case. Instead, the crossover point lies at $W_M - W_G = 0.9$ eV. Only when the graphene–metal separation is increased significantly does the crossover point decrease to its expected value, as illustrated by the upper curve for $d = 5.0$ Å in figure 6(b). This clearly demonstrates that the charge redistribution at the graphene–metal interface is not only the result of an electron transfer between the metal and the graphene levels but also due to a contribution from the chemical interaction between metal and graphene [84]. Such an interaction has been found to play an important role in describing dipole formation when closed-shell atoms and molecules are adsorbed on metal surfaces.

In addition, with further optimization using chemical functionalization a wide range of work functions can be achieved for device applications that require adjustment of the work function. Recently, to tune the work function of graphene films and thereby develop versatile electrode applications, various dipole layers were used to engineer the films and modify their surface potentials [53]. For example, when a graphene film is used as a cathode in organic devices, the work function of the graphene electrode and the lowest unoccupied molecular orbital (LUMO) of the organic functional layer must be matched to form an Ohmic contact [50, 85–87]. As illustrated in figure 6(c), the formation of dipole layers on a graphene surface should change the work function of graphene. By using different chemical materials (which can induce the dipole layer onto the graphene surface), the effective work function ($e\Phi'$) of graphene can be appropriately tuned. Figure 6(d) shows a comparison of the change in the work functions ($\Delta e\Phi$) induced by different interfacial layers [53]. The work function of the untreated graphene film was 4.58 ± 0.08 eV, which is close to the work function of highly ordered pyrolytic graphite (HOPG; 4.5 eV) [44]. The work function of the graphene film was reduced when the corresponding interfacial dipole layers were used as follows: 0.05 ± 0.03 eV with poly(ethylene oxide) (PEO), 0.22 ± 0.05 eV with Cs_2CO_3 and 0.33 ± 0.03 eV with poly[(9,9-bis((6′-(*N*,*N*,*N*-trimethylammonium)hexyl)-2,7-fluorene)-*alt*-(9,9-bis(2-(2-(2-methoxyethoxy)ethoxy)ethyl)-9-fluorene))]dibromide (WPF-6-oxy-F) [88]. For the use of graphene as a cathode electrode, WPF-6-oxy-F was found to be the best material because it reduces the effective work function of graphene to a value that is close to that of the LUMO of 1-(3-methoxycarbonyl)-propyl-1-phenyl-(6,6)C_{61} (PCBM), an active layer in organic solar cells [53].

3. Applications

3.1. Electronic devices

3.1.1. Field-effect transistors. Organic field-effect transistors (OFETs) have generated much research interest because of their low-cost fabrication, variety of materials, flexibility and wide span of potential applications [16, 89–96]. Recently, graphene has received much attention as a promising electrode material for organic electronic devices [36, 97–101]. This is due to the fact that graphene electrodes have low contact resistance because of a lower charge injection barrier to the pentacene active channel in OFETs compared to the traditional Au electrode in pentacene OFETs, as reported in our previous study [36, 102]. Therefore, it can be expected that combining the efficient charge injection afforded by graphene electrodes and the easy charge transport derived from the high ordering of the organic channel can enhance the performance of pentacene OFETs. Figure 7 shows some results of experiments using pentacene OFETs in a bottom-contact electrode device structure in which graphene films were used as the source and drain electrodes instead of a traditional metal electrode material such as Au [36]. Figure 7(b) presents the output characteristics, i.e. the drain current versus drain voltage (I_D–V_D) curves at a gate voltage (V_G) of −50 V for graphene-electrode–pentacene OFET (denoted as GR–pentacene OFET) and Au-electrode–pentacene OFET (denoted as Au–pentacene OFET) with a channel length of 50 μm. It is noteworthy that the I_D is higher for the GR–pentacene OFET than that for the Au–pentacene OFET at the same V_D and V_G values. This result indicates that the GR–pentacene OFET is superior to the Au–pentacene OFET, which is in agreement with other reports that have demonstrated the improved performance of graphene electrodes over conventional electrode (Au) [97, 98, 100]. The role of graphene electrodes as layers that provided efficient charge injection into pentacene organic channels was investigated in terms of key parameters such as contact resistance, charge injection barrier height and mobility [36]. For example, the contact resistance (R_C) can be obtained by considering the total resistance of a device (R_{tot}) versus the channel length. As summarized in figure 7(c), the R_C values of GR–pentacene OFETs were found to be smaller than those for Au–pentacene OFETs at all V_G values. Furthermore, the saturation mobilities of GR–pentacene OFETs (0.40–1.01 $cm^2\ V^{-1}\ s^{-1}$) were observed to be higher than those for Au–pentacene OFETs (0.16–0.28 $cm^2\ V^{-1}\ s^{-1}$), as

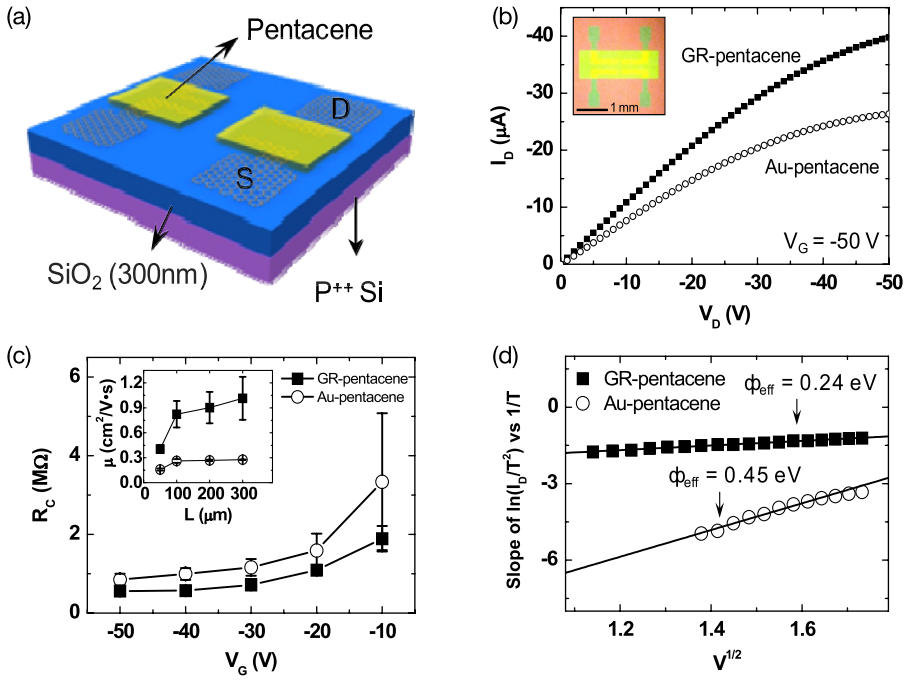

Figure 7. (a) Schematic of a graphene-electrode–pentacene OFET. (b) I_D–V_D characteristics of the GR–pentacene and Au–pentacene OFETs with a channel length of 50 μm. The inset is an optical micrograph of a fabricated GR–pentacene OFET device. (c) Contact resistance (R_C) versus gate bias (V_G) of GR–pentacene and Au–pentacene OFETs. The inset compares the saturation mobility (μ) of both types of OFETs with different channel lengths at a fixed V_G of −50 V. (d) Plots of the slopes of $\ln(I_D/T^2)$ as a function of $V_D^{1/2}$ show a linear dependence. The y-intercept value was used to deduce the effective barrier height (Φ_{eff}). Reproduced with permission from [32], Copyright 2010 Wiley-VCH.

shown in the inset of figure 7(c). This improvement in device performance originates from the improved interface properties of the graphene electrode and the pentacene channel. The R_C between the electrode and the organic channel is primarily caused by the charge injection barrier formed at the interface. Without the interfacial dipole, the hole injection barrier (Φ_h) for p-type organic semiconductors is determined by the Schottky–Mott rule, described as $\Phi_h = E_I - \Phi_m$ [103] (where E_I is the ionization energy and Φ_m is the work function). Thus, the expected injection barrier heights for GR–pentacene and Au–pentacene interfaces were determined to be 0.38 and 0.1 eV, respectively. However, this prediction contradicts the experimental observation that graphene forms better contacts (low barrier height). Such a contradiction can be explained by considering the formation of interfacial dipoles at the interface. With interfacial dipoles, the hole injection barrier is determined as $\Phi_h = E_I - \Phi_m - \Delta$ [103] (where Δ is the dipole barrier). In fact, the effective barrier height (Φ_{eff}) can be directly measured via temperature-variable I_D–V_D characterization. From the Arrhenius plots of $\ln(I_D/T^2)$ versus $1/T$ at various V_D, the slopes of these plots were used to form the plot shown in figure 7(c). From these plots, the barrier heights can be calculated from the y-intercepts of the linear fits of the data using the following thermionic emission equation [104–106]:

$$I_D = AA^*T^2 \exp\left(-\frac{q\Phi_{eff} - a\sqrt{V_D}}{k_B T}\right) \quad (2)$$

$$a = q\sqrt{\frac{q\Phi_{eff}}{4\pi\varepsilon_o\varepsilon d}} \quad (3)$$

where A is the contact area, A^* is the effective Richardson constant, k_B is the Boltzmann constant, q is the electron charge, ε_o is the permittivity of free space, ε is the dielectric constant of pentacene and d is the thickness of the pentacene film. The estimated effective barrier height using this method was ∼0.24 eV for GR–pentacene OFETs, which was significantly lower than that (∼0.45 eV) of Au–pentacene OFETs. Therefore, it was concluded that a better contact was formed in GR–pentacene than in Au–pentacene due to the favorable orientation of the interfacial dipoles at the GR–pentacene interface, which resulted in the lowering of the hole injection barrier. It is known that organic/organic interfaces form small interfacial dipoles that induce low barriers for carrier injection with respect to those of metal/organic interfaces [103, 107]. Accordingly, the graphene–pentacene interface forms a small and favorably oriented interfacial dipole layer, unlike the Au–pentacene interface which forms a significant interfacial dipole layer and results in a high carrier injection barrier [108, 109]. In addition, graphene is expected to induce strong interactions with pentacene and form excellent interfacial contact because it has a molecular structure similar to that of organic materials [98].

3.1.2. Memory devices. Recently, resistive switching in oxide-based materials as an active layer with graphene as a

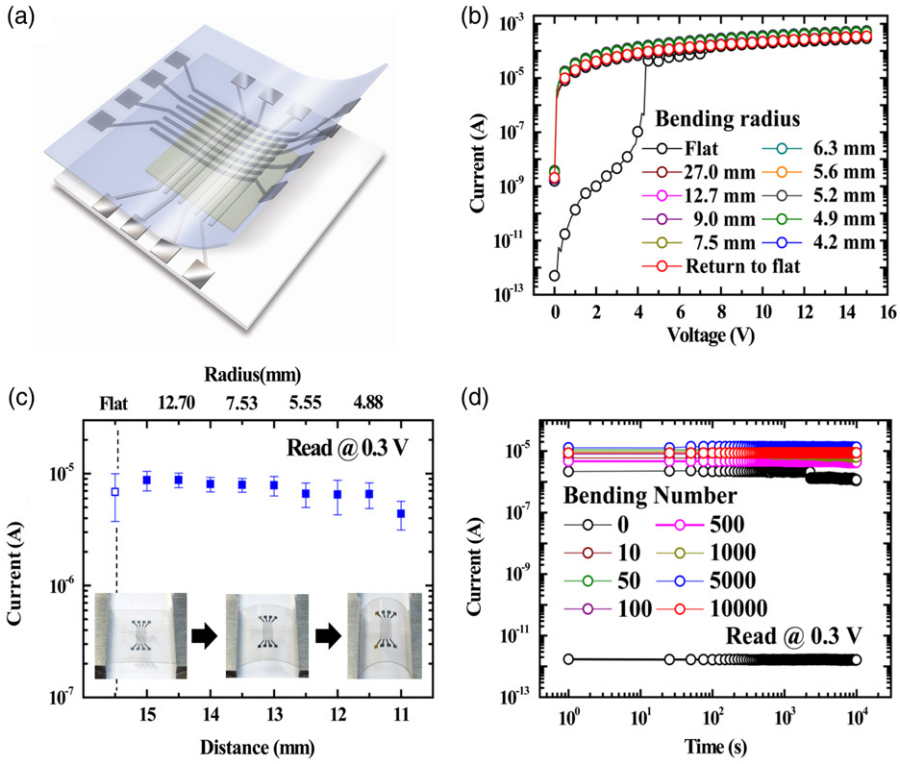

Figure 8. (a) Schematic of flexible organic memory devices consisting of PI:PCBM sandwiched between a graphene top electrode and a Al bottom electrode. (b) *I–V* characteristics of a flexible organic memory device under different bending conditions. Statistical ON current distribution of flexible organic memory devices (c) under different bending conditions and (d) for different bending cycle numbers. Reproduced with permission from [33] Copyright 2011 American Chemical Society.

conducting electrode was reported for inorganic nonvolatile memory device applications [110]. Interfacial-reaction-type resistive switching was observed upon introducing a graphene layer to electrochemically functionalize graphene at the graphene/active interface. Moreover, organic resistive memory devices with graphene electrodes have shown write-once-read-many (WORM)-type memory characteristics with good performance parameters [111]. It is expected that flexibility is required for future device applications, such as foldable and stretchable electronics. A variety of technologies have been conceived and applied to achieve flexibility in organic and inorganic electronics, and new concepts are currently being developed. In particular, the evolution of flexible electronic device applications that require information storage components has advanced research on flexible memory devices [37, 112, 113]. Unlike ITO film, which is difficult to use in flexible devices because of its brittleness under bending [10, 15, 114–117], graphene exhibits excellent durability under tension and compression [118–120]. Moreover, graphene maintains good interfacial contact with organic materials and shows a low contact resistance when combined with organic materials [97, 100]. Figure 8(a) shows a schematic of 8 × 8 array-type organic resistive memory devices with a polyimide (PI):PCBM composite solution as an active layer and graphene electrodes on a poly(ethylene terephthalate) (PET) flexible substrate [37]. The memory devices exhibited typical WORM switching characteristics, with a high ON/OFF ratio of over $\sim 10^6$ and good cell-to-cell uniformity (figure 8(b)). The ON current of the WORM memory devices did not degrade substantially upon bending cycles up to 10 000 times (figure 8(c)). A retention time of over 10^4 s was sustained by the memory devices without substantial current fluctuation under bending (figure 8(d)).

3.1.3. Molecular electronic devices. The continued miniaturization of electronics through the top-down approach is expected to reach its fundamental limit and thus has motivated significant efforts toward the development of new functional materials and devices based on self-assembled monolayer (SAM) molecules [121–126]. Molecular electronic devices have been extensively investigated through a variety of platforms and techniques in terms of understanding molecular charge transport mechanisms and potential device applications [123–125, 127, 128]. One of most widely studied molecular junctions is a solid-state device platform in which a SAM is sandwiched between two metallic electrodes [129–131]. However, this structure causes electrical short circuits and unexpected current–voltage characteristics due to filamentary paths and damage to the molecules when a metal is directly deposited on top of the molecules [130, 132]. The fabrication of molecular devices using PEDOT:PSS as an interlayer between the top electrode and SAM molecules has been one of the most successful techniques in terms of high device yields and stable junctions [129]. However, there is still a need to find alternative solid-state molecular

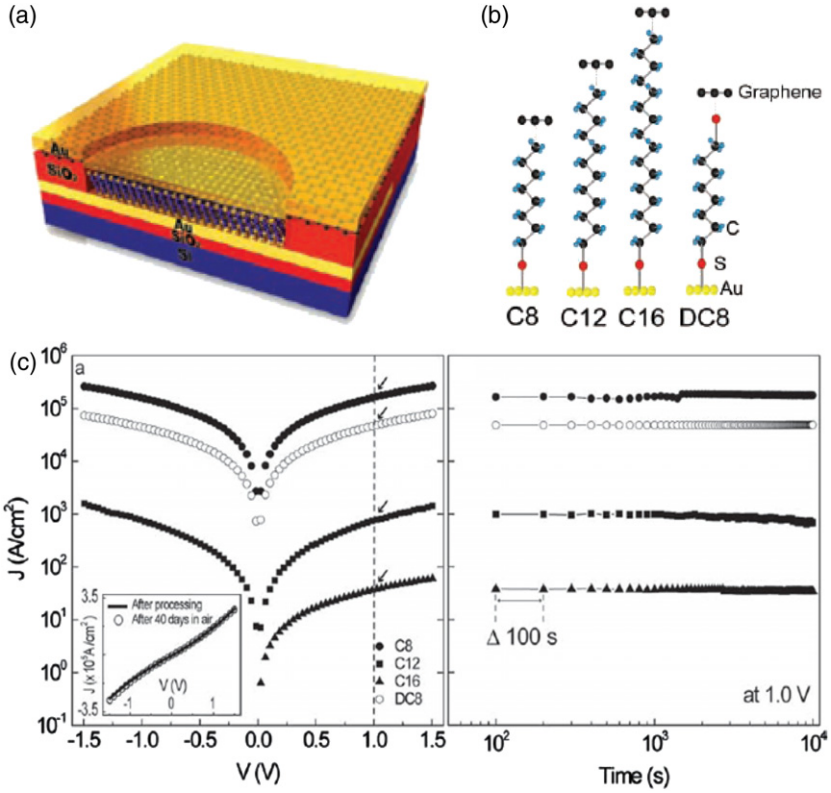

Figure 9. (a) Schematic of a graphene-based molecular electronic device. (b) Four types of studied molecular systems along with their chemical structures: C8, C12, C16 and DC8. (c) The *J–V* characteristics for representative C8, C12, C16 and DC8 graphene-electrode molecular devices. The inset shows a DC8 device measured after fabrication (solid line) and after storage under ambient conditions for 40 days (open circles). Retention characteristics of the molecular junctions in terms of the measured *J* at 1.0 V for 10^4 s (measurement interval $\Delta t = 100$ s) are shown. Reproduced with permission from [129], Copyright 2011 Wiley-VCH.

device structures beyond the PEDOT:PSS-based molecular devices because the properties of the interface between the polymer layer and the molecules are still not well understood [133]. Because graphene is an ultra-thin sheet of covalently bonded carbon atoms with promising electrical properties and chemical stability [1, 2, 134], the graphene layer between the SAM and top electrode cannot only function as a protecting layer but also forms a favorable interfacial contact. A schematic of graphene-based molecular electronic devices is shown in figure 9(a) [135]. Four types of molecular components were used for the graphene-based molecular junctions (figure 9(b)). The current-density–voltage (*J–V*) characteristics of the octanemonothiol (C8), dodecanemonothiol (C12), hexadecanemonothiol (C16) and octanedithiol (DC8) molecular junctions (the left of figure 9(c)) show good transport behavior. The *J–V* curves for a C8 junction (the inset of figure 9(c)) were measured immediately after device fabrication and after being stored under ambient conditions for 40 days, which indicates the outstanding reliability of such devices during storage in air. More interestingly, the yield of graphene-based molecular devices was found to be approximately 90%. Finally, the result for *J* at 1.0 V as a function of time showed that the operational stability was maintained for 10^4 s (the right of figure 9(c)). These results prove that a graphene interlayer can produce highly stable molecular junctions and efficiently prevent the formation of metallic filaments in molecular junctions.

3.2. Optical devices

3.2.1. Touch screen. There are a variety of touch-screen technologies, e.g. resistive, surface acoustic wave, capacitive, surface capacitance, projected capacitance [136]. Resistive and capacitive touch screens are the most common, and the electrode requirements for such applications are a sheet resistance of 300–1500 Ω/□ at a transparency of 86–90% [10]. Recently, Bae *et al* [31] have fabricated graphene films on the scale of tens of centimeters which satisfy such requirements in terms of sheet resistance and transparency. Therefore, they successfully engineered large-size graphene films into transparent electrodes, which were incorporated into touch-screen panel devices (figure 10). Using CVD, they synthesized 30-in graphene sheets on top of copper foil and were able to produce a four-ply graphene stack with 90% transparency and resistance and durability that are reportedly superior to those of ITO-based electrodes currently used in displays. The film allowed 90% of light to pass through and had an electrical resistance lower than that of the standard transparent conductor made from ITO. They also revealed that graphene outperformed ITO when they incorporated it into a real touch-screen display. ITO is used in touch screens, such as those used to record signatures when customers make a credit-card purchase. However, ITO is brittle. They showed that the

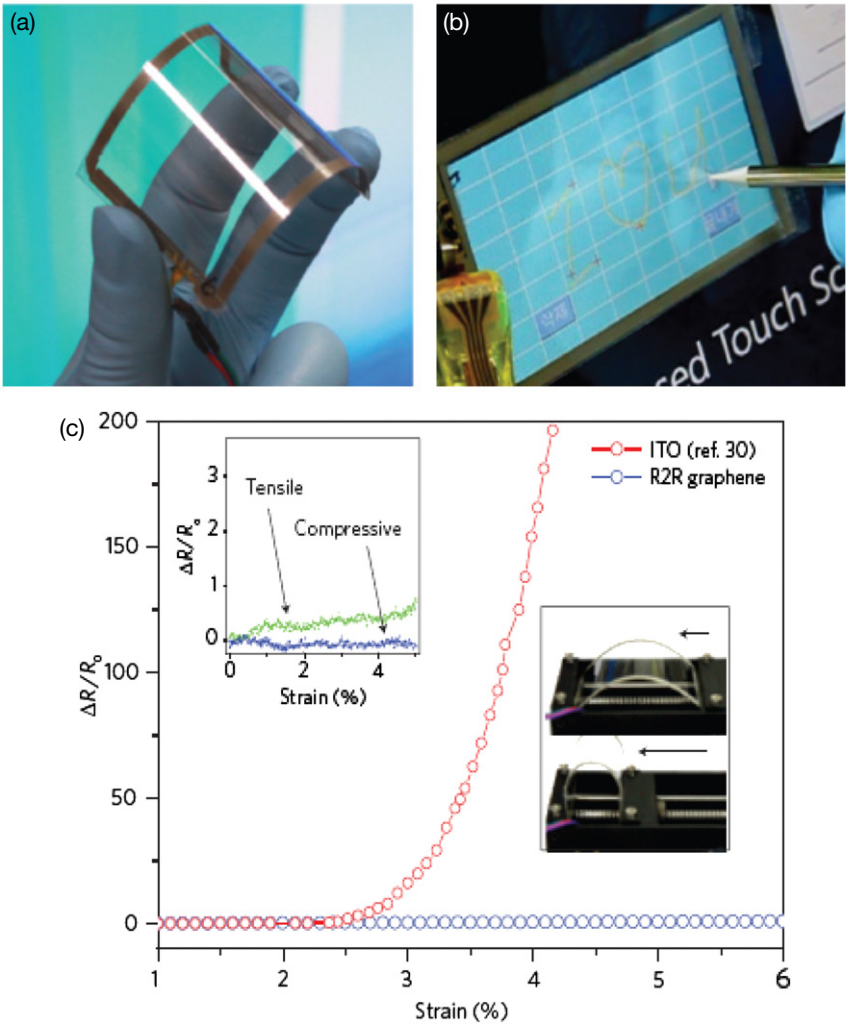

Figure 10. (a) An assembled graphene/PET touch panel showing outstanding flexibility. (b) A graphene-based touch-screen panel connected to a computer with control software. (c) Electromechanical properties of graphene-based touch-screen devices compared with ITO/PET electrodes under tensile strain. The inset shows the resistance change with compressive and tensile strain applied to graphene/PET panels. Reproduced with permission from [31], Copyright 2010 Nature Publishing Group.

graphene-based touch screen could handle twice as much strain as conventional ITO-based devices. Furthermore, the electromechanical properties of graphene/PET touch-screen panels were tested (figure 10(c)) [31]. Unlike an ITO-based touch panel, which easily breaks under 2–3% strain, the graphene-based panel resisted up to 6% strain; this is limited not by the graphene itself, but by the printed silver electrodes.

3.2.2. Liquid crystal displays. A liquid crystal display (LCD) is a flat panel display that uses the light-modulating properties of liquid crystals. It consists of thin films of optically transparent polymers with micrometer-sized liquid crystal (LC) droplets placed within pores of the polymer. Light passing through the LC polymer is strongly forward scattered, producing a milky film. If the ordinary refractive index of the LC polymer is close to that of the host polymer, the application of an electric field results in a transparent state [137]. The ability to switch from translucent to opaque states makes LCDs useful in many applications including computer monitors, televisions, instrument panels, aircraft cockpit displays, etc. A transparent conductor's major role in LCD devices is to serve as pixel and common electrodes. The electrode requirements for LCDs are rather stringent, as small as a sheet resistance of 30–300 Ω/□ at a transparency of 87–90% [10]. Recent reports also show that in the case of a 6 nm thick thermally reduced graphene oxide film, the performance of the prepared LCD device is comparable to that featuring ITO electrodes [138]. A schematic diagram of a LCD fabricated with mechanically exfoliated monolayer graphene is shown in figure 11(a) [39]. The threshold voltage of the graphene-based LCD was around 0.9 V_{rms}, and an obvious change in the transmission was observed under both white and monochromatic light (figures 11(b)–(f)). The whole graphene-electrode area changed uniformly, which suggests that the graphene has no negative effect on the liquid crystal alignment. The contrast ratio (between maximum transmission and the transmission when 100 V_{rms} is applied across the cell) was better than 100 under illumination using white light, which is outstanding for this type of cell and

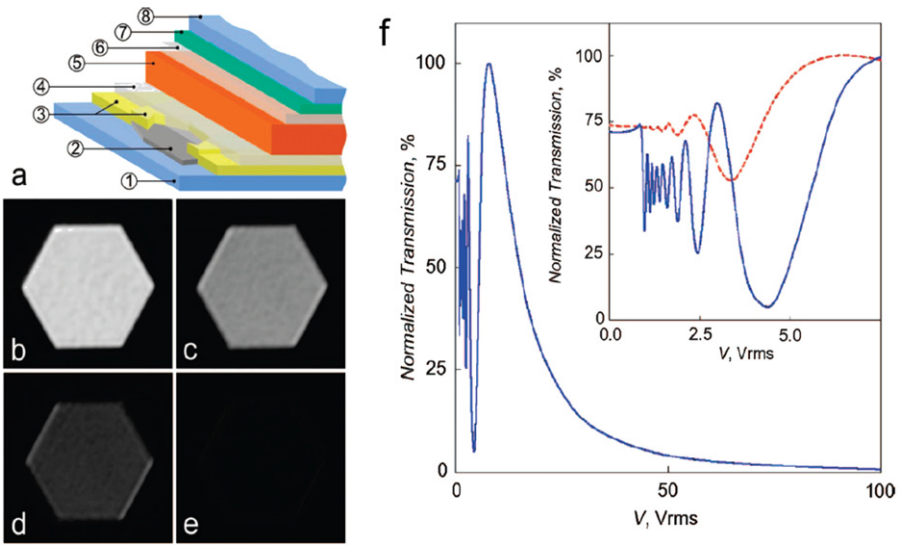

Figure 11. (a) Schematic diagram of a LCD: (1) glass (1 mm); (2) graphene; (3) Cr/Au contact surrounding graphene flake (5 nm Cr + 50 nm Au); (4) alignment layer (polyvinyl alcohol) (40 nm); (5) liquid crystal (20 μm); (6) alignment layer (40 nm); (7) ITO (150 nm); (8) glass (1 mm). (b)–(e) Optical micrographs of a LCD using green light with different voltages applied across the cell: (b) 8 V_{rms}; (c) 13 V_{rms}; (d) 22 V_{rms}; (e) 100 V_{rms}. The overall image width is 30 μm. (f) Light transmission through the LCD as a function of voltage applied across the cell. Inset: the same at low voltages. Solid blue curve: in green light (505 nm); dashed red curve: in white light. Reproduced with permission from [35], Copyright 2008 American Chemical Society.

demonstrates that graphene can indeed be used effectively as a transparent electrode for LCDs. Conventionally, ITO on glass is used as a transparent electrode to apply the electric field across an LCD. However, instability and poor flexibility hinder its further development. Another important issue for most ITO-based liquid crystal devices and other photonic devices is the chemical stability of the metal oxide and the diffusion of ions into the active medium. Such processes deteriorate the active medium via oxidation injected from ITO [139] and can lead to breakdown at lower voltages. Furthermore, in LCDs, the injected ions get trapped at the alignment layer, thus screening the applied electric field [140, 141]. One can generally expect that such issues can be prevented when using graphene, as its chemical stability should minimize the level of ion diffusion [39].

3.2.3. Light-emitting diodes. Light-emitting diodes (LEDs) have received great attention from the research and development sectors [142, 143] because LEDs can be used in flashlights and traffic signals as well as light sources in text and video displays. For example, the worldwide LCD TV market is expected to increase steadily, and LED backlights are expected to account for about 50% or more of the total number of LCD TV units (figure 1). Although the dominant material as a transparent conductor used today is still ITO, it has certain problems, mainly dramatic price fluctuations and its ceramic nature. Therefore, there is a significant need for a novel electrode material that can replace ITO in LED devices. Recently, a large-scale batch fabrication of GaN LEDs with patterned graphene as a transparent electrode was demonstrated (figure 12) [40], which is an important developmental step for more practical applications of graphene films in optoelectronic devices. In this study, a CVD-synthesized graphene film was applied as a top anode for GaN LEDs. Figure 12(f) presents the electroluminescence (EL) spectra of a fabricated multilayer graphene (MLG)-electrode GaN-based blue LED with input currents of 10, 20, 50 and 100 mA. As the input current varied from 10 to 100 mA, the EL intensity exhibited a step-up increase, indicating that the graphene electrode successfully operated as a transparent current-spreading layer over this current range. The graphene-electrode LEDs exhibited considerable performance compared to that of conventional ITO-electrode LEDs. Figure 12(g) shows the light output power versus input current characteristics of LEDs fabricated with graphene electrodes (blue filled circles) and those made with ITO (red open squares). The output power of graphene-electrode GaN LEDs continuously grew with an increase in input current up to 150 mA. At input currents below 10 mA, the output power of the graphene-electrode LEDs was comparable to that of the ITO-electrode LEDs. However, at input currents above 10 mA, the output power of the graphene-electrode LEDs was less than that of the ITO-electrode LEDs because of the higher series resistance of the graphene electrode compared to that of the ITO electrode; this higher series resistance yielded a larger voltage drop across the contact and the graphene electrode. The output power of the graphene-electrode LED was about 63% of that of the ITO-electrode LED at an input current of 20 mA. The inset of figure 12(g) compares the *I–V* characteristics of GaN LEDs with graphene and ITO electrodes. The forward voltages (defined at an input current of 20 mA) were found to be ~5.6 V and ~3.8 V for the LED with graphene and ITO electrodes, respectively. In addition, some pioneering work has reported the application of graphene thin films as transparent electrodes in organic light-emitting diodes (OLEDs) [144]. Similarly,

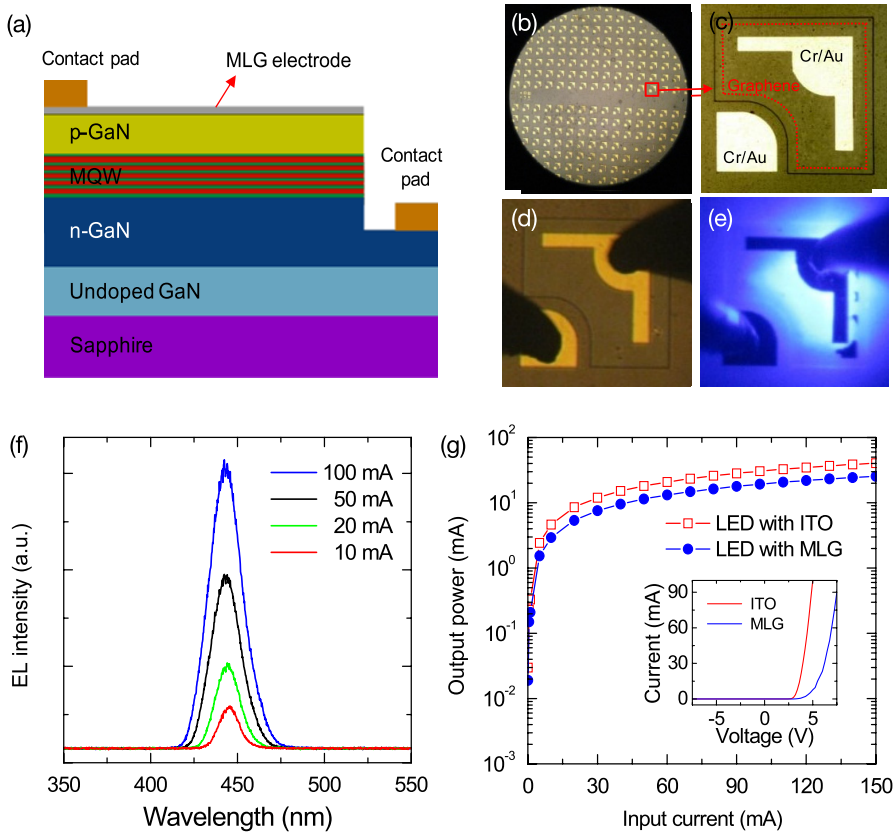

Figure 12. (a) Schematic cross-sectional view of a GaN-based LED structure with a transparent graphene electrode. (b) Large-area patterned multiple LED devices and (c) an individual LED. (d) LED with tip probes attached before applying the input current and (e) after applying an input current of 100 μA. (f) EL spectra of a GaN LED with transparent graphene electrodes at input currents of 10, 20, 50 and 100 mA. (g) Light output powers of a GaN LED with graphene electrodes (blue filled circles) and ITO electrodes (red open squares) as a function of input current. The inset shows the *I*–*V* characteristics of GaN LEDs with graphene (blue curve) and ITO (red curve) electrodes. Reproduced with permission from [36], Copyright 2010 IOP Publishing Ltd.

at high current density, the reported graphene-based OLED produced a voltage drop in the electrode due to the high sheet resistance of graphene. Further engineering of the graphene film characteristics, such as through doping, to increase the conductivity and tuning of the work function to improve the interface matching between graphene and the LED active layer will enhance the device performance of graphene-based LED/OLED devices. In addition, the chemical stability and mechanical flexibility of the transparent conductor in OLEDs is becoming indispensable. Therefore, there have been increasing demands for the development of new transparent electrode material alternatives to ITO, indicating that the research into graphene films as transparent electrodes will continue to grow.

3.2.4. Solar cells. Up to now, many kinds of graphene-based organic and inorganic solar cells have been reported in applications including dye-sensitized solar cells [44], organic bulk-heterojunction (BHJ) photovoltaic cells [43, 145], hybrid ZnO/poly(3-hexylthiophene) (P3HT) solar cells [146], Si Schottky junction solar cells [147] and InGaN p–i–n solar cells [148]. One of the reasons for the current interest in graphene arises from its potential to be used for low-cost, graphene/organic film compatibility and flexibility. Combined with the flexibility of organic molecules, this makes it potentially lucrative for graphene-based photovoltaic device applications. Arco *et al* have demonstrated highly flexible organic solar cells (OSCs) using graphene electrodes [115]. For successful implementation in these applications, however, one major challenge in developing high-performance solar cells is to effectively separate photogenerated electron–hole pairs and transfer the separated charge carriers to the electrodes. Of particular interest is the fact that graphene-based materials have demonstrated controllable surface and interfacial properties as well as tailored work functions via functionalization during synthesis and/or post-treatment [24, 53, 77]. In an organic solar cell, the difference in work function between the two conductors sets up an electric field in the organic layer. When the organic layer absorbs light, electrons will be excited to the LUMO and leave holes in the highest occupied molecular orbital (HOMO), forming excitons. The potential created by the different work functions helps to separate the exciton pairs, pulling electrons to the cathode and holes to the anode. Therefore, it is important to facilitate better transport of charge carriers to each electrode, which can be achieved by an additional functional layer. Recently, CVD-synthesized graphene films incorporated as transparent and conductive electrodes were successfully

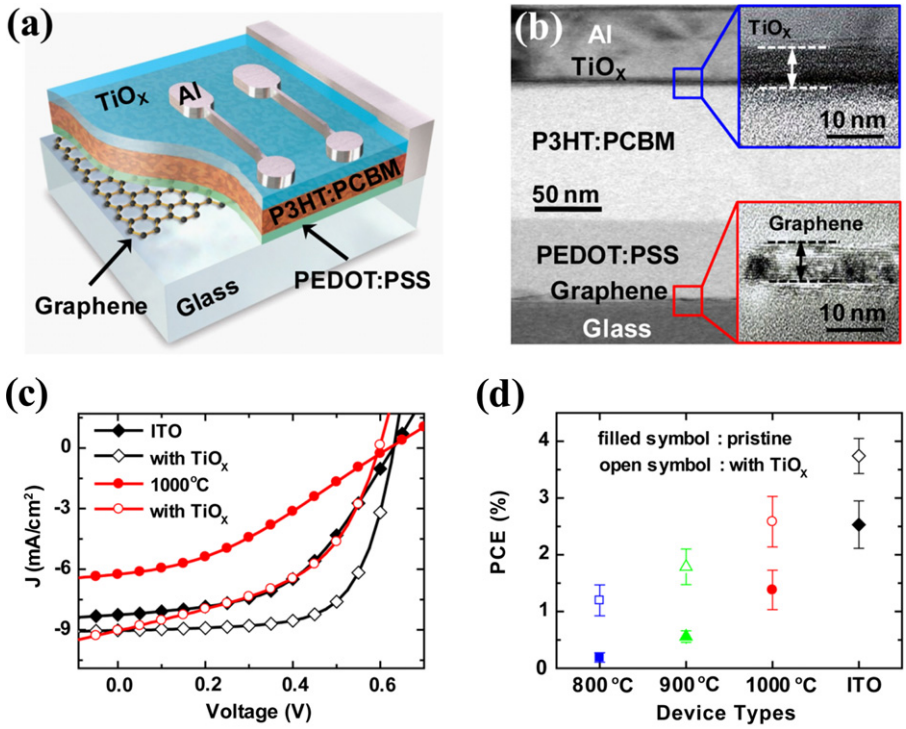

Figure 13. (a) Schematic diagram of a photovoltaic device structure with graphene electrodes and a hole-blocking TiO_X layer. (b) TEM cross-sectional image of a photovoltaic device. The insets show high-resolution TEM images near the TiO_X layer (top) and near the graphene films (bottom). (c) *J*–*V* curves of photovoltaic devices with 1000 °C-grown graphene electrodes (circles) and with ITO electrodes (diamonds). The curves without the TiO_X layer (filled symbols) are compared to those with the TiO_X layer (open symbols). (d) Comparison of the PCEs used for graphene-electrode photovoltaic devices with those used for ITO-electrode photovoltaic devices with TiO_X layers and without TiO_X layers (pristine). The types of devices are indicated on the *x*-axis (800, 900 and 1000 °C: graphene-electrode devices; ITO: ITO-electrode devices). Reproduced with permission from [39], Copyright 2010 Elsevier B.V.

applied in OSCs with a thin sol–gel-processed titanium sub-oxide (TiO_X) layer (figure 13(a)) [43]. The graphene film was transferred onto a glass substrate to form the anode for the OSCs. Then, a PEDOT:PSS layer was spin coated on top of the graphene film. The photo-active BHJ composite of P3HT and [6,6]-phenyl-C61 butyric acid methyl ester (PCBM) was spin coated on top of the PEDOT:PSS layer. Then, a TiO_X film was spin coated for some devices. Finally, aluminum was thermally evaporated to form the cathode (figure 13(b)). The growth temperature of the graphene films was studied as a control parameter on the power conversion efficiency (PCE) of the graphene-electrode OSCs. The performance of OSCs with 1000 °C-grown graphene films was found to be the best with a PCE of ∼1.3%. The PCE was further enhanced when a hole-blocking TiO_X layer was inserted in the device structure, resulting in a PCE of ∼2.6% (figures 13(c) and (d)). The enhancement of the PCE for the graphene-electrode and ITO-electrode photovoltaic devices achieved by inserting a TiO_X layer can be explained by the role the TiO_X layer plays in creating a higher density of photogenerated charge carriers as an optical spacer [149, 150] and facilitating better transport of charge carriers to each electrode as a hole-blocking layer [151, 152], thereby increasing the short-circuit current density. Moreover, the TiO_X layer reduced the contact resistance between the cathode and the P3HT:PCBM photo-active layer due to dipole formation [153]. As a result, the fill factor should be enhanced in these devices.

The PCE is the major factor in evaluating the performance of OSCs. Until now, the PCE values of graphene-electrode OSCs have been reported to be in the range of 0.08–2.60% [154], which is much lower than those of OSCs made with conventional ITO electrodes (8.37%) [155]. Therefore, the PCE of graphene-electrode OSCs needs to be much improved to make graphene film a strong candidate in OSCs.

3.3. Transparent and flexible electronics

Today, one of the most overwhelmingly popular research topics is the creation of transparent and flexible electronics for various applications: smart windows, integrated circuit (IC) cards, displays, LEDs, solar cells, and electronic paper [156, 157]. The challenge of producing invisible and bendable electronic circuitry is that all transistor components must not only be transparent to visible light but also robust under bending. To this end, the combination of optical transparency and mechanical flexibility of organic channels and graphene electrodes enables us to provide a potential solution for the realization of transparent and flexible electronic devices. Recently, transparent and flexible electronic devices such as transistors [99, 157], memory devices [37, 67] and integrated

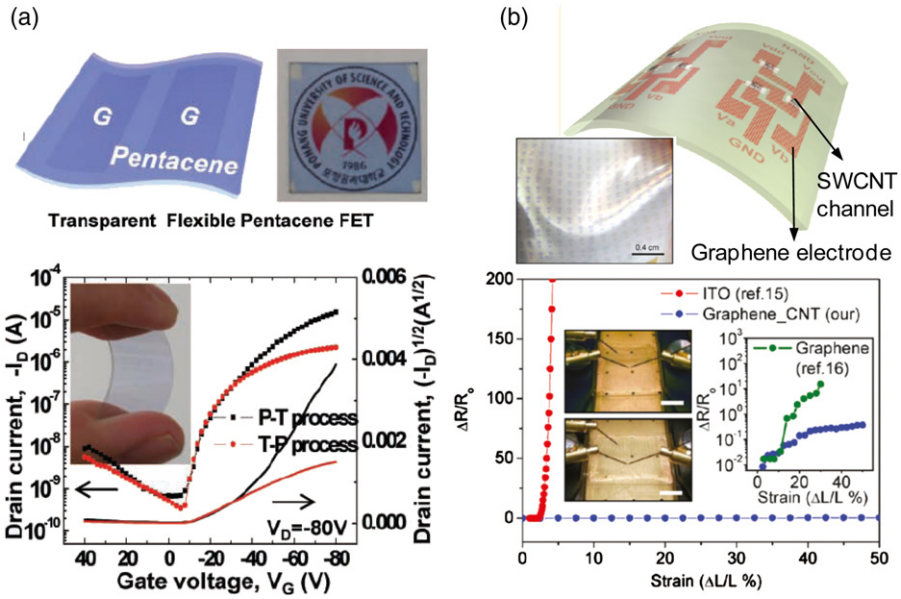

Figure 14. (a) (Upper figure) Schematic and photograph of transparent/flexible pentacene FETs with graphene source and drain electrodes. (Lower figure) Transfer characteristics of graphene-electrode-based pentacene FETs. The black and red lines were obtained by following the patterning and transfer process (P–T process) and the transfer and patterning process (T–P process), respectively. The inset shows a photograph of pentacene FETs displaying the flexible and transparent features. Reproduced with permission from [93], Copyright 2011 Wiley-VCH Verlag GmbH & Co. KGaA, Weinheim. (b) (Upper figure) Schematic of a graphene electrode and a SWCNT network channel on a flexible substrate and photograph of graphene–SWCNT FETs. (Lower figure) Resistance variation of graphene–SWCNT FETs against a strain, as compared with an ITO electrode. Left inset shows stretched images of graphene–SWCNT FET at the 0% and 50% strain. Right inset shows resistance variation, as compared with a few-layer graphene film. Reproduced with permission from [145], Copyright 2011 American Chemical Society.

circuits [157] have been demonstrated by introducing graphene electrodes and pentacene films or single-walled carbon nanotube (SWCNT) networks as active channels. Pentacene OFETs were assembled on a flexible plastic substrate by following the patterning and transfer process (P–T process) or the transfer and patterning process (T–P process) to define graphene electrodes (figure 14(a)) [99]. PEDOT/PSS, pentacene and crosslinked poly-4-vinylphenol (PVP) were used as the plastic substrate, gate electrode and gate dielectric, respectively. From the transfer characteristics of such devices shown in the lower part of figure 14(a), the field-effect mobility values of the OFETs were found to be 0.01 $cm^2\ V^{-1}\ s^{-1}$ and 0.12 $cm^2\ V^{-1}\ s^{-1}$ for the T–P process and P–T process, respectively. The OFET devices fabricated after the P–T processing of graphene films showed better performance than those after P–T processing by avoiding the damage resulting from reactive ion etching (RIE). Although transparent and flexible pentacene OFETs based on graphene electrodes were well demonstrated, the mobility should be further improved to translate into a wider range of application possibilities. Carbon nanotubes materials have been regarded as promising candidates for use in transparent and flexible electronics because they can function as semiconducting channels with fascinating electrical, mechanical and optical properties [10, 158]. Recent reports have demonstrated the fabrication of transparent and flexible transistors and logic circuits using graphene electrodes and SWCNT network channels [157], as illustrated in figure 14(b). Patterned graphene electrodes were formed on the flexible substrate by using oxygen plasma etching. Then, the gate dielectric layer (50 nm Al_2O_3) was deposited by e-beam evaporation and atomic layer deposition. Finally, SWCNT network channels were defined by oxygen plasma etching after the transfer. The devices showed favorable device performances: high mobility (81 $cm^2\ V^{-1}\ s^{-1}$), good transparency (83.8% including substrate) and excellent bending properties (no significant changes in bending 1000 times). In addition, the graphene–SWCNT FET showed only a 36% resistance variation at a 50% tensile strain unlike ITO-based FET devices (2000% resistance change at 5% strain). Therefore, graphene-electrode-based electronic devices are expected to pave the way toward the realization of advanced displays and plastic electronics with high transmittance in the near future.

4. Outlook and perspective

Graphene is a promising next-generation conducting material with the potential to replace traditional electrode materials such as metals and ITO in electrical and optical devices (figure 15). It combines several advantageous characteristics including low sheet resistance, high optical transparency and excellent mechanical properties. These properties make it an attractive candidate for application in various devices including transistors, memories, molecular junctions, touch screens, LCDs, LEDs and solar cells. Table 2 summarizes the key features of ITO and graphene and their suitability for various device applications. Many fascinating properties of graphene and its applications provide the opportunity

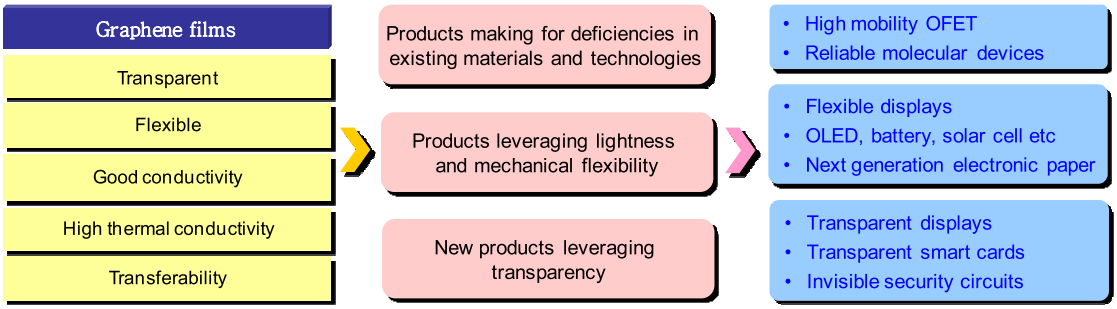

Figure 15. Outlook for graphene-based transparent electronics and optoelectronics.

Table 2. List and comparison of key features and suitability in various applications of ITO and graphene. Symbols from 'O' to 'Δ' and to 'X' mean from good to bad. '—' means it is not available in literature.

Type	ITO	Graphene
Sheet resistance (Ω/□)	Less than 100 [11, 32]	30–770 [26, 27, 31]
Transmittance (%)	∼90	∼90
Thickness (nm)	100–200 nm [159]	1.3 (4 layers) [160]
Failure strain (%)	2–3 [161]	>10 [162]
Work function (eV)	4.8 [20, 71]	4.4–4.9 [24]
Manufacturing process	Sputtering	Coating, transfer, roll to roll
Touch screen	O	O
LCD	O	O
LED	O	Δ
Solar cell	O	Δ
OFET	X	O
Memory	Δ	Δ
Molecular devices	—	O
Flexible device	X	O

to substitute graphene for ITO in transparent and flexible technologies. In electrical devices with graphene electrodes, it is possible to achieve high-performance OFETs, good resistive switching devices and highly reliable molecular junction devices due to its favorable interfacial contact with organic materials and electrochemical functionalization at the graphene/active layer interface. In addition, transparent electronics is one of the most advanced research topics that features a wide range of device applications, where the key components (i.e. electrodes, active and passive components) should be invisible. To this end, transparent metal-free transistors and circuits using graphene electrode have already been demonstrated [93, 145]. The combination of the optical transparency and mechanical flexibility of organic or carbon nanotube active channels as well as graphene electrodes makes such components attractive technologies for realizing transparent and flexible electronic devices. In optoelectronic devices (such as touch screen, LCDs, LEDs and solar cells), ITO is still the most widely used material for transparent electrodes. However, there is an increasing demand for the development of new transparent electrode materials that can challenge ITO due to ITO's cost fluctuation and brittle nature, suggesting that flexible optoelectronic devices will be an attractive market for ITO substitutes. The roll-to-roll production of CVD-grown graphene has been shown to be promising for the large-scale fabrication of transparent electrodes in flexible devices. This manufacturing-friendly technique and the high conductivity of graphene films achieved by chemical doping represent an important step toward the large-scale commercial production of transparent electrodes that may potentially replace ITO. To realize this goal in the near future, however, further research should be directed at optimizing the synthesis, transfer and doping of graphene films with the aim of attaining more conductive and low-cost graphene films. To date, there have been a vast number of reports on applications of graphene in both electrical and optical devices. We expect that future studies will include the integration of graphene-based transparent electronics with a number of other optoelectronic devices.

Acknowledgments

This work was supported by the National Research Laboratory program and a Korean National Core Research Centre grant from the Korean Ministry of Education, Science and Technology, and the Research Settlement Fund for new faculty at Seoul National University.

References

[1] Novoselov K S, Geim A K, Morozov S V, Jiang D, Zhang Y, Dubonos S V, Grigorieva I V and Firsov A A 2004 *Science* **306** 666
[2] Meric I, Han M Y, Young A F, Ozyilmaz B, Kim P and Shepard K L 2008 *Nature Nanotechnol.* **3** 654

[3] Zhang Y, Tan J W, Stormer H L and Kim P 2005 *Nature* **438** 201
[4] Chen J-H, Jang C, Xiao S, Ishigami M and Fuhrer M S 2008 *Nature Nanotechnol.* **3** 206
[5] Lee C, Wei X, Kysar J W and Hone J 2008 *Science* **321** 385
[6] Kosynkin D V, Higginbotham A L, Sinitskii A, Lomeda J R, Dimiev A, Price B K and Tour J M 2009 *Nature* **458** 872
[7] Geim A K and Novoselov K S 2007 *Nature Mater.* **6** 183
[8] Geim A K 2009 *Science* **324** 1530
[9] Wassei J K and Kaner R B 2010 *Mater. Today* **13** 52–9
[10] Hecht D S, Hu L and Irvin G 2011 *Adv. Mater.* **23** 1482
[11] Pang S, Hernandez Y, Feng X and Müllen K 2011 *Adv. Mater.* **23** 2779
[12] Bullen P and Isele R 2008 German flat panel display forum (DFF) *European Technology: Flat Panel Displays* 6th edn (Germany: VDMA)
[13] www.displaysearch.com/cps/rde/xchg/displaysearch/hs.xsl/news.asp (2011 Flat Panel TV Growth to be Half that of 2010)
[14] Fenn J 2010 'If not ITO, then what?' presented at *Soc. Vac. Coat.*
[15] 2009 *Report on 'Indium Tin Oxide and Alternative Transparent Conductor Markets' by NanoMarkets* www.nanomarkets.net.
[16] Forrest S R 2004 *Nature* **428** 911
[17] Lee J-Y, Connor S T, Cui Y and Peumans P 2008 *Nano Lett.* **8** 689
[18] De S, Higgins T M, Lyons P E, Doherty E M, Nirmalraj P N, Blau W J, Boland J J and Coleman J N 2009 *ACS Nano* **3** 1767
[19] Wu Z C *et al* 2004 *Science* **305** 1273
[20] Pasiquier A D, Unalan H E, Kanwal A, Miller S and Chhowalla M 2005 *Appl. Phys. Lett.* **87** 203511
[21] Na S I, Kim S S, Jo J and Kim D Y 2008 *Adv. Mater.* **20** 4061
[22] Chang Y M, Wang L and Su W F 2008 *Org. Electron.* **9** 968
[23] Zhu Y, Murali S, Cai W, Li X, Suk J W, Potts J R and Ruoff R S 2010 *Adv. Mater.* **22** 3906
[24] Guo C X, Guai G H and Li C M 2011 *Adv. Energy Mater.* **1** 448
[25] Kim K S, Zhao Y, Jang H, Lee S Y, Kim J M, Kim K S, Ahn J-H, Kim P, Choi J-Y and Hong B H 2009 *Nature* **457** 706
[26] Li X *et al* 2009 *Science* **324** 1312
[27] Reina A, Jia X, Ho J, Nezich D, Son H, Bulovic V, Dresselhaus M S and Kong J 2008 *Nano Lett.* **9** 30
[28] Arco L G D, Zhang Y, Kumar A and Zhou C 2009 *IEEE Trans. Nanotechnol.* **8** 135
[29] Lee Y, Bae S, Jang H, Jang S, Zhu S-E, Sim S H, Song Y I, Hong B H and Ahn J-H 2010 *Nano Lett.* **10** 490
[30] Zhu Y, Sun Z, Yan Z, Jin Z and Tour J M 2011 *ACS Nano* **5** 6472
[31] Bae S *et al* 2010 *Nature Nanotechnol.* **5** 574
[32] SPI Supplies® Brand, ITO coated microscope slides: selection of the ITO coating resistivity and thickness www.2spi.com/catalog/standards/ITO-coated-slides-resistivities5.html
[33] Hu L, Kim H S, Lee J Y, Peumans P and Cui Y 2011 *ACS Nano* **4** 2955
[34] Rinzler A G *et al* 1998 *Appl. Phys.* A **67** 29
[35] Kirchmeyer S and Reuter K 2005 *J. Mater. Chem.* **15** 2077
[36] Lee S, Jo G, Kang S-J, Wang G, Choe M, Park W, Kim D-Y, Kahng Y H and Lee T 2011 *Adv. Mater.* **23** 100
[37] Ji Y, Lee S, Cho B, Song S and Lee T 2011 *ACS Nano* **5** 5995
[38] Wang G, Kim Y, Choe M, Kim T-W and Lee T 2011 *Adv. Mater.* **23** 755
[39] Blake P *et al* 2008 *Nano Lett.* **8** 1704
[40] Jo G *et al* 2010 *Nanotechnology* **21** 175201
[41] Wu J, Agrawal M, Becerril H A, Bao Z, Liu Z, Chen Y and Peumans P 2010 *ACS Nano* **4** 43
[42] Lee J M *et al* 2010 *Nano Lett.* **10** 2783
[43] Choe M *et al* 2010 *Org. Electron.* **11** 1864
[44] Wang X, Zhi L and Müllen K 2008 *Nano Lett.* **8** 323
[45] Li X *et al* 2010 *Nano Lett.* **10** 4328
[46] Thiele S, Reina A, Healey P, Kedzierski J, Wyatt P, Hsu P-L, Keast C, Schaefer J and Kong J 2010 *Nanotechnology* **21** 015601
[47] Wei D and Liu Y 2010 *Adv. Mater.* **22** 3225
[48] Kahng Y H, Lee S, Choe M, Jo G, Park W, Yoon J, Hong W-K, Cho C-H, Lee B H and Lee T 2011 *Nanotechnology* **22** 045706
[49] Lee Y, Bae S, Jang H, Jang S, Zhu S-E, Sim S H, Song Y I, Hong B H and Ahn J-H 2010 *Nano Lett.* **10** 490
[50] Li X, Zhu Y, Cai W, Borysiak M, Han B, Chen D, Piner R D, Colombo L and Ruoff R S 2009 *Nano Lett.* **9** 4359
[51] Kim K K, Reina A, Shi Y, Park H, Li L-J, Lee Y H and Kong J 2010 *Nanotechnology* **21** 285205
[52] Guo B, Fang L, Zhang B and Gong J R 2011 *Insciences J.* **1** 80
[53] Jo G *et al* 2010 *Appl. Phys. Lett.* **97** 213301
[54] Shi Y, Kim K K, Reina A, Hofmann M, Li L-J and Kong J 2010 *ACS Nano* **4** 2689
[55] Emtsev K V, Speck F, Seyller Th and Ley L 2008 *Phys. Rev.* B **77** 155303
[56] Tung V C, Allen M J, Yang Y and Kaner R B 2009 *Nature Nanotechnol.* **4** 25
[57] Berger C *et al* 2006 *Science* **312** 1191
[58] Iyechika Y 2010 *Sci. Tech. Trends Q. Rev.* **37** 76
[59] Stankovich S, Dikin D A, Dommett G H B, Kohlhaas K M, Zimney E J, Stach E A, Piner R D, Nguyen S T and Ruoff R S 2006 *Nature* **442** 282
[60] Stankovich S, Dikin D A, Piner R D, Kohlhaas K A, Kleinhammes A, Jia Y, Wu Y, Nguyen S T and Ruoff R S 2007 *Carbon* **45** 1558
[61] Hummers W S and Offeman R E 1958 *J. Am. Chem. Soc.* **80** 1339
[62] Allen M J, Tung V C and Kaner R B 2010 *Chem. Rev.* **110** 132
[63] Tung V C, Chen L-M, Allen M J, Wassei J K, Nelson K, Kaner R B and Yang Y 2009 *Nano Lett.* **9** 1949
[64] Reina A, Thiele S, Jia X, Bhaviripudi S, Dresselhaus M S, Schaefer J A and Kong J 2009 *Nano Res.* **2** 509
[65] Chae S J *et al* 2009 *Adv. Mater.* **21** 2328
[66] Park S and Ruoff R S 2009 *Nature Nanotechnol.* **4** 217
[67] Yu W J, Chae S H, Lee S Y, Duong D L and Lee Y H 2011 *Adv. Mater.* **23** 1889
[68] Li X *et al* 2009 *Science* **324** 1312
[69] Becerril H A, Mao J, Liu Z, Stoltenberg R M, Bao Z and Chen Y 2008 *ACS Nano* **2** 463
[70] Eda G, Fanchini G and Chhowalla M 2008 *Nature Nanotechnol.* **3** 270
[71] Gordon R G 2000 *MRS Bull.* **25** 52–7
[72] Nistor R A, Newns D M and Martyna G J 2011 *ACS Nano* **5** 3096
[73] Gierz I, Riedl C, Starke U, Ast C R and Kern K 2008 *Nano Lett.* **8** 4603
[74] Huh S, Park J, Kim K S, Hong B H and Kim S B 2011 *ACS Nano* **5** 3639
[75] Yu Y-J, Zhao Y, Ryu S, Brus L E, Kim K S and Kim P 2009 *Nano Lett.* **9** 3430
[76] Giovannetti G, Khomyakov P A, Brocks G, Karpan V M, Brink J v d and Kelly P J 2008 *Phys. Rev. Lett.* **101** 026803
[77] Huang J-H, Fang J-H, Liu C-C and Chu C-W 2011 *ACS Nano* **5** 6262
[78] Wang X, Li X, Zhang L, Yoon Y, Weber P K, Wang H, Guo J and Dai H 2009 *Science* **324** 768
[79] Wang Y, Shao Y, Matson D W, Li J and Lin Y 2010 *ACS Nano* **4** 1790
[80] Wei D, Liu Y, Wang Y, Zhang H, Huang L and Yu G 2009 *Nano Lett.* **9** 1752

[81] Wu Z-S, Ren W, Xu L, Li F and Cheng H-M 2011 *ACS Nano* **5** 5463
[82] Park H, Rowehl J A, Kim K K, Bulovic V and Kong J 2010 *Nanotechnology* **21** 505204
[83] Yu Y-J, Zhao Y, Ryu S, Brus L E, Kim K S and Kim P 2009 *Nano Lett.* **9** 3430
[84] Giovannetti G, Khomyakov P A, Brocks G, Karpan V M, Brink J v d and Kelly P J 2008 *Phys. Rev. Lett.* **101** 026803
[85] Chen L-M, Hong Z, Li G and Yang Y 2009 *Adv. Mater.* **21** 1434
[86] Ma H, Yip H-L, Huang F and Jen A K-Y 2010 *Adv. Funct. Mater.* **20** 1371
[87] Zhang F, Ceder M and Inganäs O 2007 *Adv. Mater.* **19** 1835
[88] Oh S-H, Na S-I, Jo J, Lim B, Vak D and Kim D-Y 2010 *Adv. Funct. Mater.* **20** 1977
[89] Lee T-W, Byun Y, Koo B-W, Kang I-N, Lyu Y-Y, Lee C H, Pu L and Lee S Y 2005 *Adv. Mater.* **17** 2180
[90] Artukovic E, Kaempgen M, Hecht D S, Roth S and Grüner G 2005 *Nano Lett.* **5** 757
[91] Horowitz G 1998 *Adv. Mater.* **10** 365
[92] Wu Y, Li Y, Gardner S and Ong B S 2005 *J. Am. Chem. Soc.* **127** 614
[93] Yan H, Chen Z, Zheng Y, Newman C, Quinn J R, Dötz F, Kastler M and Facchetti A 2009 *Nature* **457** 679
[94] Aguirre C M, Ternon C, Paillet M, Desjardins P and Martel R 2009 *Nano Lett.* **9** 1457
[95] Zhang Y Y, Shi Y, Chen F, Mhaisalkar S G, Li L-J, Ong B S and Wu Y 2007 *Appl. Phys. Lett.* **91** 223512
[96] Lefenfeld M, Blanchet G and Rogers J A 2003 *Adv. Mater.* **15** 1188
[97] Pang S, Tsao H N, Feng X and Müllen K 2009 *Adv. Mater.* **21** 3488
[98] Di C-A, Wei D, Yu G, Liu Y, Guo Y and Zhu D 2008 *Adv. Mater.* **20** 3289
[99] Lee W H, Park J, Sim S H, Jo S B, Kim K S, Hong B H and Cho K 2011 *Adv. Mater.* **23** 1752
[100] Lee C-G, Park S, Ruoff R S and Dodabalapur A 2009 *Appl. Phys. Lett.* **95** 023304
[101] Park J, Lee W H, Huh S, Sim S H, Kim S B, Cho K, Hong B H and Kim K S 2011 *J. Phys. Chem. Lett.* **2** 841
[102] Lee S *et al* 2011 *Appl. Phys. Lett.* **99** 083306
[103] Ishii H, Sugiyama K, Ito E and Seki K 1999 *Adv. Mater.* **11** 605
[104] Chen J, Calvet L C, Reed M A, Carr D W, Grubisha D S and Bennett D W 1999 *Chem. Phys. Lett.* **313** 741
[105] Nam C Y, Tham D and Fischer J E 2005 *Nano Lett.* **5** 2029
[106] Weis M, Nakao M, Lin J, Manaka T and Iwamoto M 2009 *Thin Solid Films* **518** 795
[107] Lee C-G, Park S, Ruoff R S and Dodabalapur A 2009 *Appl. Phys. Lett.* **95** 023304
[108] Diao L, Frisbie C D, Schroepfer D D and Ruden P P 2007 *J. Appl. Phys.* **101** 014510
[109] Amy F, Chan C and Kahn A 2005 *Org. Electron.* **6** 85
[110] Lee W *et al* 2011 *Appl. Phys. Lett.* **98** 032105
[111] Liu J, Yin Z, Cao X, Zhao F, Lin A, Xie L, Fan Q, Boey F, Zhang H and Huang W 2010 *ACS Nano* **4** 3987
[112] Jeong H Y *et al* 2010 *Nano Lett.* **10** 4381
[113] Son D I, Kim T W, Shim J H, Jung J H, Lee D U, Lee J M, Park W I and Choi W K 2010 *Nano Lett.* **10** 2441
[114] Forrest S R 2004 *Nature* **428** 911
[115] Arco L G D, Zhang Y, Schlenker C W, Ryu K, Thompson M E and Zhou C 2010 *ACS Nano* **4** 2865
[116] Lee B H, Park S H, Back H and Lee K 2011 *Adv. Funct. Mater.* **21** 487
[117] Boehme M and Charton C 2005 *Surf. Coat. Technol.* **200** 932
[118] Frank O, Tsoukleri G, Parthenios J, Papagelis K, Riaz I, Jalil R, Novoselov K S and Galiotis C 2010 *ACS Nano* **4** 3131
[119] Tsoukleri G, Parthenios J, Papagelis K, Jalil R, Ferrari A C, Geim A K, Novoselov K S and Galiotis C 2009 *Small* **5** 2397
[120] Yu T, Ni Z, Du C, You Y, Wang Y and Shen Z 2008 *J. Phys. Chem.* C **112** 12602
[121] Nitzan A and Ratner M A 2003 *Science* **300** 1384
[122] Love J C, Estroff L A, Kriebel J K, Nuzzo R G and Whitesides G M 2005 *Chem. Rev.* **105** 1103
[123] Chen J, Reed M A, Rawlett A M and Tour J M 1999 *Science* **286** 1550
[124] Reed M A, Zhou C, Muller C J, Burgin T P and Tour J M 1997 *Science* **278** 252
[125] Green J E *et al* 2007 *Nature* **445** 414
[126] Behin-Aein B, Datta D, Salahuddin S and Datta S 2010 *Nature Nanotechnol.* **5** 266
[127] Lafferentz L, Ample F, Yu H, Hecht S, Joachim C and Grill L 2009 *Science* **323** 1193
[128] Kushmerick J G, Holt D B, Yang J C, Naciri J, Moore M H and Shashidhar R 2002 *Phys. Rev. Lett.* **89** 086802
[129] Akkerman H B, Blom P W M, de Leeuw D M and de Boer B 2006 *Nature* **441** 69
[130] Kim T-W, Wang G, Lee H and Lee T 2007 *Nanotechnology* **18** 315204
[131] Wang W, Lee T, Kretzschmar I and Reed M A 2004 *Nano Lett.* **4** 643
[132] Walker A V, Tighe T B, Cabarcos O M, Reinard M D, Haynie B C, Uppili S, Winograd N and Allara D L 2004 *J. Am. Chem. Soc.* **126** 3954
[133] Nijhuis C A, Reus W F and Whitesides G M 2009 *J. Am. Chem. Soc.* **131** 17814
[134] Wang Q H and Hersam M C 2009 *Nature Chem.* **1** 206
[135] Wang G, Kim Y, Choe M, Kim T-W and Lee T 2011 *Adv. Mater.* **23** 755
[136] Bonaccorso F, Sun Z, Hasan T and Ferrari A C 2010 *Nature Photon.* **4** 611
[137] Sheraw C D *et al* 2002 *Appl. Phys. Lett.* **80** 1088
[138] Nordendorf G, Kasdorf O, Kitzerow H S, Liang Y, Feng X and Muellen K 2010 *Japan. J. Appl. Phys.* **49** 100206
[139] Scott J C, Kaufman J H, Brock P J, DiPietro R, Salem J and Goitia J A 1996 *J. Appl. Phys.* **79** 2745
[140] Bremer M, Naemura S and Tarumi K 1998 *Japan. J. Appl. Phys.* **37** L88
[141] Schlatmann A R, Floet D W, Hilberer A, Garten F, Smulders P J M, Klapwijk T M and Hadziioannou G 1996 *Appl. Phys. Lett.* **69** 1764
[142] Chichibu S F *et al* 2006 *Nature Mater.* **5** 810
[143] Chamings J, Ahmed S, Sweeney S J, Odnoblyudov V A and Tu C W 2008 *Appl. Phys. Lett.* **92** 021101
[144] Wu J, Agrawal M, Becerril H c A, Bao Z, Liu Z, Chen Y and Peumans P 2010 *ACS Nano* **4** 43
[145] Li S S, Tu K H, Lin C C, Chen C W and Chhowalla M 2010 *ACS Nano* **4** 3169
[146] Yin Z, Wu S, Zhou X, Huang X, Zhang Q, Boey F and Zhang H 2010 *Small* **2** 307
[147] Li X, Zhu H, Wang K, Cao A, Wei J, Li C, Jia Y, Li Z, Li X and Wu D 2010 *Adv. Mater.* **22** 2743
[148] Shim J-P, Choe M, Jeon S-R, Seo D, Lee T and Lee D-S 2011 *Appl. Phys. Express* **4** 052302
[149] Kim J Y, Kim S H, Lee H-H, Lee K, Ma W, Gong X and Heeger A J 2006 *Adv. Mater.* **18** 572
[150] Roy A, Park S H, Cowan S, Tong M H, Cho S, Lee K and Heeger A J 2009 *Appl. Phys. Lett.* **95** 013302
[151] Park S H, Roy A, Beaupre S, Cho S, Coates N, Moon J S, Moses D, Leclerc M, Lee K and Heeger A J 2009 *Nature Photon.* **3** 297

[152] Kim J Y, Lee K, Coates N E, Moses D, Nguyen T-Q, Dante M and Heeger A J 2007 *Science* **317** 222
[153] Cho S, Seo J H, Lee K and Heeger A J 2009 *Adv. Funct. Mater.* **19** 1459
[154] Wan X, Long G, Huang L and Chen Y 2011 *Adv. Mater.* **23** 5342
[155] He Z, Zhong C, Huang X, Wong W, Wu H, Chen L, Su S and Cao Y 2011 *Adv. Mater.* **23** 4636
[156] Wager J F 2003 *Science* **300** 23
[157] Yu W J, Chae S H, Lee S Y, Duong D L and Lee Y H 2011 *Nano Lett.* **11** 1344
[158] Jo G, Hong W-K, Sohn J I, Jo M, Shin J, Welland M E, Hwang H, Geckeler K E and Lee T 2009 *Adv. Mater.* **21** 2156
[159] Wong F L, Fung M K, Tong S W, Lee C S and Lee S T 2004 *Thin Solid Films* **466** 225
[160] Ni Z H, Wang H M, Kasim J, Fan H M, Yu T, Wu Y H, Feng Y P and Shen Z X 2007 *Nano Lett.* **7** 2758
[161] Cairns D R, Witte R P, Sparacin D K, Sachsman S M, Paine D C, Crawford G P and Newton R R 2000 *Appl. Phys. Lett.* **76** 1425
[162] Lee C, Wei X, Kysar J W and Hone J 2008 *Science* **321** 385

Dear readers,

I would like to let you know that this paper has incorrect information on Refs. # in Figure captions (2, 4-9, 11-14). Refs. # in text are correct, but there are 17 errors in Figure captions. Please see the list below.

1. On page 3, in Figure 2(a) caption
"… Reproduced with permission from [51], …" should be as "… Reproduced with permission from [55], …"
2. On page 3, in Figure 2(c) caption
"… Reproduced with permission from [52], …" should be as "… Reproduced with permission from [56], …"
3. On page 5, in Figure 4(a,b) caption
"… (a), (b) Reproduced with permission from [36], …" should be as "… Reproduced with permission from [40], …"
4. On page 5, in Figure 4(c,d) caption
"… (c), (d) Reproduced with permission from [39], …" should be as "… Reproduced with permission from [43], …"
5. On page 5, in Figure 5(a) caption
"… Reproduced with permission from [66], …" should be as "… Reproduced with permission from [72], …"
6. On page 5, in Figure 5(b) caption
"… Reproduced with permission from [75], …" should be as "… Reproduced with permission from [81], …"
7. On page 6, in Figure 6(a) caption
"… Reproduced with permission from [77], …" should be as "… Reproduced with permission from [75], …"
8. On page 6, in Figure 6(b) caption
"… Reproduced with permission from [78], …" should be as "… Reproduced with permission from [76], …"
9. On page 6, in Figure 6(d) caption
"… Reproduced with permission from [49], …" should be as "… Reproduced with permission from [53], …"
10. On page 8, in Figure 7 caption
"… Reproduced with permission from [32], …" should be as "… Reproduced with permission from [36], …"
11. On page 9, in Figure 8 caption
"… Reproduced with permission from [33], …" should be as "… Reproduced with permission from [37], …"
12. On page 10, in Figure 9 caption
"… Reproduced with permission from [129], …" should be as "… Reproduced with permission from [135], …"
13. On page 12, in Figure 11 caption
"… Reproduced with permission from [35], …" should be as "… Reproduced with permission from [39], …"
14. On page 13, in Figure 12 caption
"… Reproduced with permission from [36], …" should be as "… Reproduced with permission from [40], …"
15. On page 14, in Figure 13 caption
"… Reproduced with permission from [39], …" should be as "… Reproduced with permission from [43], …"
16. On page 15, in Figure 14(a) caption
"… Reproduced with permission from [93], …" should be as "… Reproduced with permission from [99], …"
17. On page 15, in Figure 14(b) caption
"… Reproduced with permission from [145], …" should be as "… Reproduced with permission from [157], …"

I apologize for the inconvenience caused to you. Please feel free to contact me, if you have any problem and question.

Best regards,

Gunho Jo
E-mail: gunhojo@princeton.edu
Phone: 1-609-759-1933